

Morphological and imaging evaluation of the metacarpophalangeal and metatarsophalangeal joints in healthy and lame donkeys.

Samir A.A. El-Gendy^{a*}, Mohamed A.M. Alsafy^a, Catrin Sian Rutland^{b*}, Ahmad N. EL-Khamary^c, Howaida M. Abu-Ahmed^d and Mahmoud H. El-Kammar^d

^aDepartment of Anatomy and Embryology, Faculty of Veterinary Medicine, Alexandria University, Egypt.

^bSchool of Veterinary Medicine and Science, Faculty of Medicine, University of Nottingham, UK.

^cDepartment of Surgery, Faculty of Veterinary Medicine, Damanshour University, Egypt

^dDepartment of Surgery, Faculty of Veterinary Medicine, Alexandria University, Egypt

*Corresponding authors: elgendyanatomist@yahoo.com and catrin.rutland@nottingham.ac.uk

elgendyanatomist@yahoo.com Dr. Samir E-Gendy.

safy73@yahoo.com Dr. Mohamed Alsafy

Catrin.rutland@nottingham.ac.uk Dr. Catrin Rutland

ahmed.nasr@damanhour.edu.eg Dr. Ahmad El-Khamary

Howaida_maf@yahoo.com Dr. Howida Abou-Ahmed

m_elkammar2010@yahoo.com Dr. Mahmoud El-Kammar

Highlights

Anatomical description of donkey metacarpophalangeal and metatarsophalangeal joints

Pathologies observed in clinically abnormal donkey joints including exostosis

New anatomical structures observed in donkey joints

Optimized computed tomography methodology can give better visualization for soft tissues

Abstract

The donkey is of socio-economic value yet imaging techniques in both healthy and abnormal limbs are a limiting factor in research and medicine. The objective was to determine anatomical features of both healthy and clinically abnormal donkey metacarpophalangeal and metatarsophalangeal joints (n=13) using anatomical dissection, casting, x-ray and computed tomography. The joint capsule contained two palmar/plantar and two dorsal recesses. The proximal-palmar or plantar recess was larger than the distodorsal recess and potential sites of approaches to the recesses were determined. Soft tissue structures were distinguished using computed tomography at 300mA which was superior to 120mA. This methodology gave better assessments of the synovial tendon sheath, joint recesses and cruciate, collateral and short sesamoidean ligaments. Computed tomography provided outstanding discrimination between the cortex and medulla of the third metacarpal, the proximal sesamoid bones, the proximal phalanx and excellent details of the osseous structures. Although the joints appeared free from exostosis using x-ray; the position and extension of exostosis in pathologically affected donkeys (a novel finding) was revealed using computed tomography with 300mA in comparison to 120mA. The study also provided an anatomical record of the metacarpophalangeal and metatarsophalangeal joints using the latest technology which could impact on clinical situations including anesthesia injection sites.

Keywords:

50 Computed tomography; Radiography; Exostosis; Lameness.

51

52

53 **1. Introduction**

54 The metacarpophalangeal and metatarsophalangeal joints (fetlock joint) have received
55 considerable critical attention because of their anatomical complexity and are the joints most
56 frequently affected by degenerative and traumatic lesions in the equine species [1, 2] causing
57 a high incidence of lameness. Therefore understanding their anatomy and identifying these
58 problems is essential. Current imaging techniques have their limitations in relation to viewing
59 the joint. In cases such as early cartilage loss and subchondral bone injury, radiography and
60 scintigraphy are not always able to detect changes, especially in cases without marked
61 structural bone damage or demineralization. In contrast, evaluation of bone lesions and joint
62 structures may be more appropriate using computed tomography as it provides 3-dimensional
63 images, attenuation coefficient values through windows and tissue density in Hounsfield units
64 [1, 3-6]. Computed tomography can also be useful in understanding orthopedic diseases,
65 during pre-surgical planning and in disease progression prevention. On the other hand soft
66 tissue evaluation with CT can be improved with the use of contrast agents but is often
67 considered inferior to magnetic resonance imaging [6]. It has been demonstrated [7] that
68 using higher tube currents and voltages and thicker sections significantly enhances the
69 accuracy of detection of low-contrast objects. Therefore, it is essential to optimize the factors
70 that could improve image quality in both clinical and research settings to ensure that artifacts
71 and lesions are correctly identified and interpreted.

72 Donkeys are the tenth most numerous domesticated mammals in the world [8, 9], with
73 an estimated 41 million donkeys supporting 600 million people worldwide [10, 11]. The
74 present study describes the main anatomical structures of the donkey metacarpophalangeal
75 and metatarsophalangeal joints. The hypothesis was that computed tomography undertaken at
76 a high mA would give better images than a lower mA in relation to the metacarpophalangeal
77 and metatarsophalangeal joint, especially when visualizing soft tissue structures.

78 Comparisons between x-rays and computed tomography were also made. The second
79 hypothesis was that limbs from lame animals would show differing anatomical structures
80 when compared to healthy limbs. The third hypothesis was that the anatomical structures of
81 the donkey would not differ from those of the horse. The donkey is good for studying equine
82 pathophysiological orthopedic processes, because of its very close phylogenetically,
83 biomechanically and biochemically properties in comparison with the horse [12-14] therefore
84 differences in comparison to the published anatomy of the horse are also discussed. The study
85 also identified new bone growth and pathologies in donkeys with metacarpophalangeal and
86 metatarsophalangeal joint problems. This study presents valuable, clinically relevant,
87 information for anatomical training and research, anesthesia, medicine, surgery in this
88 important animal which is relevant in other animals including the horse.

89

90

91 **2. Material and Methods**

92 **2.1 Animals and ethics**

93 All four limbs from thirteen adult donkeys of both sexes were used with age matched controls
94 (aged 5-8 years, Table 1). Nomenclature observes Nomina Anatomica Veterinaria
95 terminology [15]. Each donkey (n=13) and their corresponding health records were
96 independently assessed by two specialist donkey and equine lameness veterinary surgeons
97 who confirmed 'healthy' or 'non-healthy' metacarpophalangeal and metatarsophalangeal
98 joints (Table 1). The following criteria were used: Non-healthy animals had a history of
99 metacarpophalangeal/metatarsophalangeal joint trauma and lameness, which was chronic at

100 the time of investigation with light to moderate (grades 1-2) degrees of lameness which
101 increased after trotting. Animals suspected to have joint effusion with synovial proliferation
102 and osteoarthritic changes based on manual examination (inspection, palpation, passive
103 movement of joints) were also considered 'non-healthy'. 'Healthy' donkeys required a life
104 history and veterinary examination free from deformities/lameness/trauma and study scans
105 further confirmed each diagnosis.

106 This study followed the guidelines for the care and use of animals and approved by
107 the Animal Welfare and Ethics Committees of the Alexandria University, Damanhur
108 University and The University of Nottingham (ethical number 2173 171214). No animals
109 were euthanized specifically for research purposes. Euthanasia was undertaken under general
110 anesthesia by veterinary surgeons via intravenous injection of 10mg/kg thiopental sodium
111 (EPICO, Egypt) after premedication with 1mg/kg xylazine hydrochloride (Xylaject; Egypt).

112 **2.2 Study Design**

113 **2.2.1 Anatomical dissection and cast**

114 Four male and female clinically healthy donkeys free from joint pathology were used.
115 Following euthanasia the animals were bled from the common carotid artery.
116 Metacarpophalangeal and metatarsophalangeal joints from each animal were used (one left
117 forelimb and one right hind limb per animal). The joint cavity of one limb was injected with
118 gum milk latex (Sudan) mixed with a red dye (Carmine Alum Lake, USA) before dissection.
119 One donkey (one metacarpophalangeal and one metatarsophalangeal joint) underwent routine
120 preservative and fixation techniques (10% formalin:4% glycerin:1% phenol; two weeks) prior
121 to dissection. These techniques provided gross anatomical specimens to compliment imaging
122 techniques (Fig. 1+ 4).

123 **2.2.2 Computed radiography**

124 Five healthy and five non-healthy donkeys with chronic joint pathology underwent computed
125 radiography (Table 1). Furthermore, one donkey joint was injected with contrast medium via
126 the palmar recess to further investigate the palmar/plantar recesses. Images were captured on
127 a phosphor plate using Toshiba 500MA fixed x-ray machine, output of 60Kv and 10mA. The
128 time was adjusted automatically with the mA, images were digitally processed using a CR
129 reader (R30-X. Agfa, Japan). Five standard radiographic views were used for each joint,
130 (dorsopalmar, lateromedial, flexed lateromedial, dorso45°lateral-palmaromedial oblique, and
131 dorsomedial-palmarolateral oblique views with an angle of 45°).

132 **2.2.3 Computed tomography**

133 Five donkeys with joint pathology and two healthy donkeys, all previously used for
134 radiography, were euthanized and the limbs severed at carpal/tarsal joints. Computed
135 tomography protocols (multislice helical computed tomography scanner, Toshiba Astesion
136 Super 4 Edition) were used to obtain 1mm thick scan slices at currents of 120kV and 120mA
137 (lower mA) and 300mA (higher mA). Collimation was at 0.75mm with 4mm reconstruction
138 interval, 1 second rotation time, field of view of 32cm and a pitch of 1.05-2. The matrix size
139 was 512×512 pixels. Both bone (window width 3000, window level 700) and soft tissue
140 (window width 300, window level 80) windows were used. Limbs were placed in the gantry
141 with the long axis of the limb parallel to the table. Limbs were scanned in a distal to proximal
142 direction beginning from proximal aspect of first phalanx and continuing to 2cm above the
143 distal aspect of third metacarpal bone. Specimens underwent bone and soft tissue windows
144 scanning in transverse, sagittal and dorsal planes.

145

146

147 **3. Results**

148 **3.1 Gross anatomy of the metacarpophalangeal and metatarsophalangeal joints**

149 The articular surfaces of the metacarpophalangeal and metatarsophalangeal joints were
150 comprised of the third metacarpal/metatarsal bone, the proximal phalanx and the paired
151 proximal sesamoid bones. The distal epiphysis of the third metacarpal/metatarsal bone
152 consisted of two condyles separated by a sagittal ridge; the medial condyle was the largest
153 (Figs.2+5+Supplemental Figure 1). The proximal extremity of the proximal phalanx
154 consisted of two articular cavities, the medial cavity slightly larger than the lateral one
155 (Fig.2). The two proximal sesamoid bones had a three sided pyramid shape, their dorsal
156 surfaces articulated with the condyles of the large metacarpal/metatarsal bone (Figs.1+2).

157 The ligaments of the metacarpophalangeal and metatarsophalangeal joints were the
158 collateral ligaments and sesamoidean apparatus. The medial and lateral collateral ligaments
159 had superficial and deep parts (Fig.1). The sesamoidean apparatus included the suspensory,
160 collateral, straight, oblique, short and cruciate sesamoidean, and intersesamoidean ligaments.
161 The suspensory ligament presented on the palmar surface of the large metacarpal bone
162 between the two splint bones (Fig.1). The suspensory ligament divided into two diverging
163 branches attached to the abaxial surface of the corresponding proximal sesamoid bone. Then
164 the extensor branch of suspensory ligament passed obliquely distally and dorsally to the
165 dorsal surface of the proximal phalanx, where it attached to the common digital extensor
166 tendon or long digital extensor tendon in the hind limb (Fig.1). The lateral and medial
167 collateral sesamoidean ligaments united the proximal sesamoid bones to the metacarpus
168 proximally and to the proximal phalanx distally (Fig.1). The straight sesamoidean ligament
169 originated from the proximal sesamoid bones and inserted on the palmar border of the base of
170 the proximal phalanx and to the tuberositas flexoria of the second phalanx (Fig.1) covered on
171 the plantar or palmar side by the superficial and deep digital flexor tendon and related tendon
172 sheath. The oblique sesamoidean ligament was narrow in width proximally, wider distally,
173 originating from the base of the proximal sesamoid bones and adjacent part of the
174 intersesamoidean ligament to the distal fourth of the palmar surface of the proximal phalanx
175 (Fig.1). The cruciate sesamoidean ligament included two bands of tissue located across the
176 distopalmar recess of the joint. The fibers of each strand were attached proximally to the base
177 of the respective proximal sesamoid bone and adjacent part of the intersesamoidean ligament.
178 They extended obliquely towards the opposite palmar tubercle on the base of the proximal
179 phalanx. The intersesamoidean ligament was represented by a narrow dense
180 fibrocartilaginous mass which filled the space between the adjacent proximal sesamoid bones
181 (Fig.1). The short sesamoidean ligaments consisted of short bands from the base of the
182 proximal sesamoid bone to the palmar border of the base of the proximal phalanx (Fig.1).
183 The related structures of fetlock joint included the superficial digital flexor tendon, the deep
184 digital flexor tendon and the digital sheath which extended from above the fetlock joint to the
185 middle of the middle phalanx. The sheath enclosed the deep digital flexor tendon, partially
186 surrounding the superficial digital flexor tendon.

187 The joint capsule appeared to be capacious and attached around the articular surfaces
188 consisting of fibrous and synovial layers. The capsule formed four recesses; two palmar or
189 plantar and two dorsal recesses. The proximal-palmar recess was larger and the smaller one
190 presented as a distodorsal recess. The dorsoproximal recess extended for 1.5-2cm on the third
191 metacarpal bone (Fig.1). The small distodorsal recess (Figs.1,2+4) was narrow and a smaller
192 section of the dorsal recess reached 2-3mm from the distal region to the articular surface of
193 the first phalanx and related dorsally by the common digital extensor tendon and
194 dorsolaterally by lateral extensor tendon. Access to the dorsal recess was possible both
195 medially and laterally to the tendon of the long digital extensor muscle, the medial route was
196 more accessible. The palmar recess had thin walls and was located between the distal
197 extremity of third metacarpal bone and the suspensory ligament until its bifurcation;
198 proximally, it was covered by the suspensory ligament, superficial and deep digital flexor

199 tendons. The palmar recess formed a main palmaroproximal recess under the suspensory
200 ligament, and a palmarodistal recess under the straight sesamoidean ligament and cruciate
201 sesamoidean ligaments (Figs.1-4). The approach to the dorsal palmar recess was performed
202 with the limb held in a flexed position and by palpating the triangle depression between
203 suspensory ligament the third metatarsal/tarsal bone and lateral proximal sesamoid bone.

204 **3.2 Computed radiography**

205 The dorsopalmar radiographs of the metacarpophalangeal and metatarsophalangeal joints
206 were approximately symmetrical about the prominent sagittal ridge of the distal metacarpus,
207 the medial condyle was slightly wider than the lateral. The sagittal ridge articulated with a
208 groove in the proximal phalanx. The joint space was observed to be at right angles to the long
209 axis of the third metacarpal bone. The proximal sesamoid bones superimposed on the third
210 metacarpal/metatarsal bone and highlighted the axial and abaxial borders of the bone
211 (Fig.2A). The dorsopalmar view allowed good visualization of the joint space and condyles
212 of the distal third metacarpal/metatarsal. The lateromedial radiographs of the joints showed
213 the condyles of the third metacarpal/metatarsal bone and proximal sesamoid bones
214 superimposed on each other and the joint space was identifiable. The joint surface of the
215 distal metacarpal/metatarsal condyle was smooth and curved. In the lateromedial view only
216 the dorsal and palmar/plantar aspects were visualized (Fig.2B). The flexed lateromedial
217 radiographs highlighted specific areas of the joint, especially the distal aspect of the sagittal
218 ridge, which was less opaque and more dorsally located than the medial and lateral condyles,
219 and elevated the proximal sesamoid bones away from the joint surface. It also enabled
220 visualization of the dorsal-palmar and palmarodistal recesses of the joint (Fig.2C) and of the
221 entire articular surfaces of the proximal sesamoid bones and of the sagittal ridge of the
222 metacarpal/metatarsal bones in comparison to standard lateromedial and dorsopalmar
223 projections. The dorsolateral-palmaromedial oblique and dorsomedial-palmarolateral oblique
224 views highlighted the lateral sesamoid and dorsomedial aspects of the joint or medial
225 sesamoid and dorsolateral aspects of the joint respectively.

226 In addition to showing the features of the normal limb, x-rays were used to investigate
227 the non-healthy limbs in which new bone projections were extensive and radiodense growths
228 varied in shape and size along the apical and basilar portions of the proximal sesamoid. Two
229 cases of metacarpophalangeal joint sesamoiditis were accompanied by calcification of the
230 suspensory ligament which appeared as mineralized opacities superimposed on suspensory
231 ligaments (Fig.3A+B).

232

233 **3.3 Computed tomography**

234 The bone windows clarify the bone of the distal extremity of metacarpal and metatarsal
235 bones, diaphysis and sagittal ridges of third metacarpal/metatarsal bones, the condyles, the
236 proximal sesamoid bones and the proximal phalanx were seen on transverse and sagittal
237 images (Fig.5+Supp Fig 2). All images had obvious delineation between the cortex and
238 medulla of the bones and had smooth outlines and homogenous contours. The soft structures
239 such as ligaments, tendons and synovial sheath were homogeneously hypodense, visualization
240 was difficult using this window. The soft tissue window with transverse and sagittal planes
241 identified the common extensor tendon, dorsal extensor tendon, superficial digital flexor
242 tendon, deep digital flexor tendon and digital sheath cavity (Fig. 5+Supp Fig 2),
243 intersesamoidean ligament, straight and oblique sesamoidean ligaments. Medial and lateral
244 branches of suspensory ligament were the same density as the intersesamoidean ligament and
245 were difficult to recognize in this study and were therefore not discussed further.

246 Computed tomography at 120kV and 300mA: The bone window usage on the sagittal
247 images showed a comprehensive evaluation of the sagittal ridge contour, proximal sesamoid
248 bone and condyles of the two joint extremities (Supp Fig 2). All images showed excellent

249 delineation between the cortex, medulla of bone and provided more detail about the bone
250 density and thickness of the subchondral bone of the distal condyles of the third
251 metacarpal/metatarsal bones (Fig.6). The soft tissue window with transverse and sagittal
252 plans identified; suspensory ligament branches, extensor branches of the suspensory
253 ligament, superficial and deep digital flexor tendons, common digital extensor tendon,
254 straight, oblique, and cruciate sesamoidean ligaments, intersesamoidean ligament and the
255 collateral ligaments (Fig.6 +Supp Fig 2) respectively. The proximal, distal synovial tendon
256 sheath (the recesses of the digital sheath (cavity)) were best visualized on sagittal and
257 transverse images, as a thin hypodense rim surrounding the deep digital flexor tendon
258 (Fig.6+Supp Fig 2) and the four joint recesses were recognizable. Cruciate sesamoidean
259 ligaments were evaluated better using a longitudinal rather than transverse view. Collateral
260 sesamoidean ligaments and short sesamoidean ligaments could also be identified using
261 transverse views (Fig.6).

262 **3.4 Computed tomography of the abnormal metacarpophalangeal and** 263 **metatarsophalangeal joints.**

264 The usage of transverse computed tomography bone windows of the abnormal
265 metacarpophalangeal joints at 120kV and 120mA at different levels of the sesamoid bone and
266 dorsopalmar view showed a bony projection (bone exostosis) which was thin and curved
267 medially. X-ray views made it difficult to determine positions and directions of the exostosis,
268 whilst computed tomography bone window images gave more information enabling
269 determination of the position and direction of even small/thin exostosis (Fig.7). The bony
270 exostosis was observed in four of the five non-healthy donkeys.

271 Soft window transverse and sagittal computed tomography images were also used to
272 look at the abnormal metatarsophalangeal joints at 120kV and 300mA (Fig.8). The soft
273 window transverse computed tomography images of the abnormal metatarsophalangeal joint
274 at the level proximal to, and at the level of, the sesamoid bone, show an increased joint cavity
275 size and appearance of a hyperdense transverse septum. There was a septum presented at the
276 palmar recess with obvious demarcation of synovial fluid (synovitis). There was an abnormal
277 wave like shape appearance of the superficial digital extensor tendon, however this could
278 have been an artifact due to dissection and should be studied in further in live animals. In
279 addition, changes in density and appearance of the fluid at the suspensory apparatus were
280 observed.

281

282

283

283 **4. Discussion**

284

285

286

287

288

289

290

291

292

293

294

295

296

297

298

The present study identified anatomical features in both the healthy and abnormal metacarpophalangeal and metatarsophalangeal joints in donkeys using complementary imaging techniques. The morphological structures of the articular surfaces within the metacarpophalangeal and metatarsophalangeal joints of the donkey and ligaments of the joints bear resemblances to those published in the literature about horses [16-18]. One major difference was that the donkey joint capsule formed a dorsal recess which had a large dorsal and small distodorsal recess, whilst the palmar or plantar recess consisted of dorsal-ventral parts, these structures have not been observed in the publications pertaining to the horse.

Radiographic exam is sensitive enough to identify consistent lesions with proliferative synovitis and osteoarthritis [19, 20] and is the most used imaging tools for the diagnosis of bone disorders affecting the metacarpophalangeal and metatarsophalangeal joints [1, 19, 21, 22]. The current study indicated the importance of flexed lateromedial radiographs giving better depictions of the articular surfaces of the proximal sesamoid bones and sagittal ridge of the metacarpal/metatarsal bone. This provided more accurate localization of lesions and better morphology of these structures, including osteochondritis of the distal sagittal ridge

299 which has not previously been observed and/or erroneously diagnosed as cystic lesions [1,
300 22]. The lateromedial view allowed good visualization of the palmar/plantar aspect of
301 condyles of the distal third metacarpal/metatarsal, base of the proximal sesamoid bones and
302 first/proximal phalanx [19, 21]. The dorsopalmar view enabled good visualization of joint
303 spaces and condyles of the distal third metacarpal/metatarsal bone. So most condylar
304 fractures are best visualized on that projection revealing an abaxial and proximal
305 displacement [19, 23]. The dorsolateral-palmaromedial and dorsomedial-palmolateral 45°
306 oblique views allowed assessment of the shape, internal architecture and the apex, dorsal,
307 palmar and distal borders of the lateral and medial proximal sesamoid bones respectively. It
308 was also required to highlight individual proximal sesamoid bones because standard views
309 allowed only partial visualization of these structures [21] (Fig.2D+E). The 45° oblique views
310 were better for evaluating the regions of insertion of the suspensory ligament branch on the
311 abaxial surface of the proximal sesamoid bone. It also allowed assessment of the medial and
312 lateral palmar process of the proximal phalanx and the dorsomedial and dorsolateral aspects
313 aspect of the joint respectively. Based on the results of the current study, it is recommended
314 that intraarticular anesthesia/medication of the metacarpophalangeal and metatarsophalangeal
315 joints in donkeys is performed via the three traditional approaches used in horses; the dorsal
316 recess, palmar/plantar recess or through the collateral ligament of the proximal sesamoid
317 bone. The latter approach is favored by most practitioners [24] and is performed with the
318 limb held in a flexed position with the needle directed perpendicularly to the palpable
319 depression between the third metatarcapal/tarsal bone and lateral proximal sesamoid bone at
320 the level of proximal aspect of the collateral ligament of the joint.

321 Two chronic lesions with new bone proliferation, sesamoditis and calcification of
322 suspensory ligament, were diagnosed using radiography and elicited a pain response on
323 palpation. With four of the five unhealthy animals showing exostosis which was not observed
324 in the healthy animals or described in the literature to date, this matter warrants further
325 investigation. Whether these growths developed in response to limb complications or caused
326 the lameness in these animals is yet to be established. It is possible they are secondary to
327 chronic pathology in the digital sheath and some may reflect chronic tendon lesions which
328 have mineralised. Differing theories in relation to inflammation, acute trauma, prolonged
329 exposure to lameness, microfractures in the bone stimulating bone redevelopment and the
330 extra bone growth itself increasing levels of lameness could all be possible reasons for the
331 exostosis or lameness observed. There is a growing body of evidence to suggest that
332 lameness is strongly associated with extra bone/cartilage proliferation and growth. Bovine
333 lameness has been associated with extra bone growth on the caudal aspect of the distal
334 phalanx [25] and on or around the flexor tuberosity with age [26]. Humans also have extra
335 bone growth such as ‘bony spur formation’ and enthesopathy including calcification and
336 irregular bone profiles in relation to activities such as increased mechanical load and exercise
337 in addition to a number of limb, endocrine and metabolic disorders [27, 28]. Exostosis in
338 horses has also been linked to lameness including on the metacarpal and metatarsal bones and
339 the radius [29-31],

340
341 Computed tomography provided a comprehensive evaluation of the contour of the
342 sagittal ridge, proximal sesamoid bone and condyles of two extremities forming the joint,
343 especially using bone windows at 120kV and 300mA. Moreover, all images showed excellent
344 delineation between the cortex, medulla of bone and provided more details about the
345 thickness and bone density of the subchondral bone of the distal condyles of the third
346 metacarpal/metatarsal bones. Several published studies discuss the superiority of computed
347 tomography over the radiography for the diagnosis and understanding the underlying
348 pathological change in osteoarthritis [32-34] condylar fracture [35, 36] and third metacarpal

349 palmar condyle disease [34]. This superiority in the evaluation of the metacarpophalangeal
350 and metatarsophalangeal joints is due to the complex anatomical arrangement of the joint
351 with the superimposition of the sesamoid bones and the distal third metacarpal and
352 first/proximal phalanx. Additionally computed tomography provided highly detailed cross-
353 sectional and three-dimensional images, making it superior for some clinical evaluations.

354 Computed tomography evaluation of subchondral bone is crucial for early diagnosis
355 of injury, and helps to explain the possible causes of lameness without classic clinical or
356 radiographic changes or positive intraarticular blocking. Failure of intra-articular anesthesia
357 to alleviate subchondral bone pain is problematic [37-40]. Cartilage damage has a later onset
358 and the pain emanates from subchondral bone [41], 30-50% of the bone can be lost prior to it
359 being identified radiographically [42, 43]. Therefore, computed tomography can yield better
360 anatomic orientations of the subchondral bone and provide a more sensitive detection and
361 characterization of osteolysis and osteogenesis than conventional radiographs and more
362 importantly prior to clinically significant effects [42, 43]. This is also an important factor to
363 consider when assessing exostosis as observed in the abnormal limbs in this study. The
364 present study showed that CT images were more sensitive and comprehensive when detecting
365 exostosis than conventional radiographs. The difficulties in showing exostosis specificity and
366 severity in horses has been highlighted in previous studies using radiography and
367 ultrasonography [31].

368 Details of the soft tissue in computed tomography have previously been inferior to
369 magnetic resonance imaging [16, 44]. The present study highlighted that in addition to bone
370 structures being observed, clinically important soft tissue structures may be identified better
371 by adjusting the tube current to 300mA instead of 120mA, however further studies are
372 required to fully investigate this. With image thickness and kilovoltage held constant, a
373 reduction in tube current increases image noise but decreases radiation exposure, so there is a
374 tradeoff between image quality and radiation dosage [45]. Likewise, increasing tube current
375 leads to increased radiation exposure and decreased image noise, but lesions may be obscured
376 by higher noise levels [46-49]. It has also been reported that 'image noise' can be improved
377 by using a higher tube current, because it is inversely proportional to the square root of the
378 photon flux [7]. Consistent with these theories, the contrast-to-noise ratio and the confidence
379 level of low-contrast phantom detection were enhanced by increasing tube voltage and tube
380 current. With section thickness set at 10mm, the contrast-to-noise ratio increased from 0.8
381 obtained at 400mAs and 120kVp, to 1.0 at a tube current and voltage of 450mAs and
382 135kVp, respectively. However irradiation doses increase with current increases therefore
383 caution is advised in the clinical setting, highlighting an area of future research. Future
384 research expanding the number of donkeys and the types of limb disorders, which were
385 limitations of the study, would also benefit this area. A full investigation into the types and
386 locations of the exostosis in differing limb disorders would enhance the knowledge about the
387 types of abnormalities and potentially inform diagnosis and treatment in addition to under the
388 basic biological mechanisms underlying the exostosis. This would include the use of imaging
389 techniques but also histological and molecular and cellular techniques in order to fully
390 understand the mechanisms behind the growth. As the horse is so closely related to the
391 donkey, a comparative study of the two animals would provide a unique insight into lameness
392 disorders.

393

394 **5. Conclusions**

395 This study has shown the anatomy of the normal and lameness affected metacarpophalangeal
396 and metatarsophalangeal joints in the donkey, identified differences between the structures
397 and highlighted clinically important information in relation to potential sites of injection and
398 imaging. This included not only new anatomical structures but also exostosis which was

399 present in animals with a history of lameness but not in those with healthy limbs. Anatomical
400 knowledge is essential not only for present clinical procedures but also for emerging
401 treatments including gene therapy [50]. We have also shown that optimized computed
402 tomography enabled more precise evaluation of bone lesions and metacarpophalangeal and
403 metatarsophalangeal joint adjacent structures and developed of protocols for clinical and
404 research practice.

405

406 **Conflict of Interest:**

407 Declarations of interest: none

408

409 **List of Author Contributions**

410 **Samir A.A. El-Gendy:** Conception and Design, Acquisition of Data, Analysis and
411 Interpretation of Data, Drafting the Article, Revising Article for Intellectual Content, Final
412 Approval of the Completed Article. **Mohamed A.M. Alsafy:** Analysis and Interpretation of
413 Data, Drafting the Article, Final Approval of the Completed Article. **Catrin S. Rutland:**
414 Analysis and Interpretation of Data, Drafting the Article, Revising Article for Intellectual
415 Content, Final Approval of the Completed Article. **Ahmad N. EL-Khamary:** Acquisition of
416 Data, Analysis and Interpretation of Data, Drafting the Article, Final Approval of the
417 Completed Article. **Howaida M. Abu-Ahmed:** Acquisition of Data, Analysis and
418 Interpretation of Data, Drafting the Article, Final Approval of the Completed Article.
419 **Mahmoud H. El-Kammar:** Conception and Design, Acquisition of Data, Analysis and
420 Interpretation of Data, Drafting the Article, Revising Article for Intellectual Content, Final
421 Approval of the Completed Article.

422

423 **Acknowledgements**

424 Funding was kindly provided by Alexandria University, Damanhur University and The
425 University of Nottingham. Funding sources had no other involvement in the study.

426

427

428

429 [1] Machado VMV, Aguiar ACS, Viana GF, Crosignani NO, Puoli JNP. Diagnostic value of
430 computed tomography, radiography and ultrasonography in metacarpophalangeal joint
431 disorders in horses. *Arq Bras Med Vet Zoo.* 2016;68:66-72.

432 [2] Ross MW, Dyson SJ. *Diagnosis and management of lameness in the horse.*
433 Philadelphia, USA.: Elsevier-Saunders.; 2003.

434 [3] Amin M, Elbakary RMA, Alsafy MAM, Fathi n. Radiographic and Computed
435 Tomographic Anatomy of the Fetlock, Pastern and Coffin joints of the Manus of the
436 Donkey (*Equus asinus*). *Alexandria J Vet Sci.* 2014;41:68-79.

437 [4] Badawy M. Computed Tomographic Anatomy of the Fore Foot in One-Humped
438 Camel. *Glob Vet.* 2011;6:417-23.

439 [5] Groth AM, May SA, Weaver MP, Weller R. Intra- and interobserver agreement in the
440 interpretation of navicular bones on radiographs and computed tomography scans.
441 *Equine Vet J.* 2009;41:124-9.

442 [6] Widmer WR, Buckwalter KA, Fessler JF, Hill MA, VanSickle DC, Ivancevich S. Use of
443 radiography, computed tomography and magnetic resonance imaging for evaluation of
444 navicular syndrome in the horse. *Vet Radiol Ultrasoun.* 2000;41:108-16.

445 [7] Tanaka C, Ueguchi T, Shimosegawa E, Sasaki N, Johkoh T, Nakamura H, et al. Effect of
446 CT acquisition parameters in the detection of subtle hypoattenuation in acute cerebral
447 infarction: a phantom study. *AJNR Am J Neuroradiol.* 2006;27:40-5.

- 448 [8] Swai ES, Bwanga SJR. Donkey keeping in northern Tanzania: socio-economic roles
449 and reported husbandry and health constraints. *Livestock Res Rural Dev.* 2008;20:1-97.
- 450 [9] Wilson RT. The past, present and future of domestic equines in Tanzania. *J Equine*
451 *Sci.* 2013;24:37-45.
- 452 [10] McKenna C. *Bearing a Heavy Burden.* London, UK.: The Brooke.; 2007.
- 453 [11] Waltraud K., Grunenfelder HP, Broxham E. *Donkey Breeds in Europe: Inventory,*
454 *St.Gallen, Switzerland: Monitoring Institute for Rare Breeds and Seeds in Europe;* 2008.
- 455 [12] Elmesiry A., Seleim M, Cullis-Hill D. Iodoacetate and allogeneous cartilage particles
456 as models for arthritis induction in equine. *Int J Vet Sci Med.* 2014;2:142-50.
- 457 [13] Mokbel AN, El Tookhy OS, Shamaa AA, Rashed LA, Sabry D, El Sayed AM. Homing
458 and reparative effect of intra-articular injection of autologous mesenchymal stem cells in
459 osteoarthritic animal model. *BMC Musculoskelet Disord.* 2011;12:259.
- 460 [14] Singh KI, Sobti VK, Roy KS. Gross and histomorphological effects of therapeutic
461 ultrasound (1 WATT/CM²) in experimental acute traumatic arthritis in donkeys. *J*
462 *Equine Vet Sci.* 1997;17:150-5.
- 463 [15] (I.C.V.G.A.N) ICoVGAN. *Nomina Anatomica Veterinaria.* 6th ed: WAVA; 2017.
- 464 [16] Vanderperren K, Ghaye B, Snaps FR, Saunders JH. Evaluation of computed
465 tomographic anatomy of the equine metacarpophalangeal joint. *Am J Vet Res.*
466 2008;69:631-8.
- 467 [17] Dyce KM, Sack WO, Wensing CJG. *Textbook of veterinary anatomy: Elsevier Health*
468 *Sciences;* 2009.
- 469 [18] Gottschalk R. The equine distal limb: An atlas of clinical anatomy and comparative
470 imaging (7th impression). *J S Afr Vet Assoc.* 2011;82:253.
- 471 [19] Vanderperren K, Saunders JH. Diagnostic imaging of the equine fetlock region using
472 radiography and ultrasonography. Part 2: The bony disorders. *Vet J.* 2009;181:123-36.
- 473 [20] Park RD. Optimal radiographic views for evaluating thoroughbred yearlings -
474 quality control of the radiographic image. 46th Annual Convention of the American
475 Association of Equine Practitioners San Antonio, Texas, USA. 2000. p. 357-8.
- 476 [21] Butler JA, Colles CM, Dyson SJ, Kold SE, Poulos PW. *Clinical Radiology of the Horse.*
477 3rd. ed. Oxford, UK.: Blackwell Science; 2011.
- 478 [22] Wright IM, Minshall GJ. Identification and treatment of osteochondritis dissecans of
479 the distal sagittal ridge of the third metacarpal bone. *Equine Vet J.* 2014;46:585-8.
- 480 [23] Vanderperren K, Saunders JH. Diagnostic imaging of the equine fetlock region using
481 radiography and ultrasonography. Part 1: Soft tissues. *Vet J.* 2009;181:111-22.
- 482 [24] Misheff MM, Stover SM. A comparison of two techniques for arthrocentesis of the
483 equine metacarpophalangeal joint. *Equine Vet J.* 1991;23:273-6.
- 484 [25] Newsome R, Green MJ, Bell NJ, Chagunda MGG, Mason CS, Rutland CS, et al. Linking
485 bone development on the caudal aspect of the distal phalanx with lameness during life. *J*
486 *Dairy Sci.* 2016;99:4512-25.
- 487 [26] Tsuka T, Ooshita K, Sugiyama A, Osaki T, Okamoto Y, Minami S, et al. Quantitative
488 evaluation of bone development of the distal phalanx of the cow hind limb using
489 computed tomography. *J Dairy Sci.* 2012;95:127-38.
- 490 [27] Benjamin M, Toumi H, Ralphs JR, Bydder G, Best TM, Milz S. Where tendons and
491 ligaments meet bone: attachment sites ('entheses') in relation to exercise and/or
492 mechanical load. *J Anat.* 2006;208:471-90.
- 493 [28] Slobodin G, Rozenbaum M, Boulman N, Rosner I. Varied presentations of
494 enthesopathy. *Semin Arthritis Rheum.* 2007;37:119-26.

495 [29] Bertoni L, Forresu D, Coudry V, Audigie F, Denoix JM. Exostoses on the palmar or
496 plantar aspect of the diaphysis of the third metacarpal or metatarsal bone in horses: 16
497 cases (2001-2010). *J Am Vet Med Assoc.* 2012;240:740-7.

498 [30] Zubrod CJ, Schneider RK, Tucker RL. Use of magnetic resonance imaging to identify
499 suspensory desmitis and adhesions between exostoses of the second metacarpal bone
500 and the suspensory ligament in four horses. *Javma-J Am Vet Med A.* 2004;224:1815-+.

501 [31] Zetterstrom SM, Johansson BC, Carmalt JL. Evaluation of clinical and tenoscopic
502 findings in the carpal flexor sheath of horses. *Am J Vet Res.* 2017;78:840-6.

503 [32] Messent EA, Ward RJ, Tonkin CJ, Buckland-Wright C. Tibial cancellous bone
504 changes in patients with knee osteoarthritis. A short-term longitudinal study using
505 Fractal Signature Analysis. *Osteoarthr Cartilage.* 2005;13:463-70.

506 [33] Messent EA, Ward RJ, Tonkin CJ, Buckland-Wright C. Cancellous bone differences
507 between knees with early, definite and advanced joint space loss; a comparative
508 quantitative macroradiographic study. *Osteoarthr Cartilage.* 2005;13:39-47.

509 [34] Muir P, Peterson AL, Sample SJ, Scollay MC, Markel MD, Kalscheur VL. Exercise-
510 induced metacarpophalangeal joint adaptation in the Thoroughbred racehorse. *J Anat.*
511 2008;213:706-17.

512 [35] Delguste C, Amory H, Guyonnet J, Thibaud D, Garnero P, Detilleux J, et al.
513 Comparative pharmacokinetics of two intravenous administration regimens of
514 tiludronate in healthy adult horses and effects on the bone resorption marker CTX-1. *J*
515 *Vet Pharmacol Ther.* 2008;31:108-16.

516 [36] Dore F, Filippi L, Biasotto M, Chiandussi S, Cavalli F, Di Lenarda R. Bone
517 scintigraphy and SPECT/CT of bisphosphonate-induced osteonecrosis of the jaw. *J Nucl*
518 *Med.* 2009;50:30-5.

519 [37] Dyson S. Problems associated with the interpretation of the results of regional and
520 intra-articular anaesthesia in the horse. *Vet Rec.* 1986;118:419-22.

521 [38] Niv D, Gofeld M, Devor M. Causes of pain in degenerative bone and joint disease: a
522 lesson from vertebroplasty. *Pain.* 2003;105:387-92.

523 [39] Sampson SN, Schneider RK, Tucker RL, Gavin PR, Zubrod CJ, Ho CP. Magnetic
524 resonance imaging features of oblique and straight distal sesamoidean desmitis in 27
525 horses. *Vet Radiol Ultrasound.* 2007;48:303-11.

526 [40] Schumacher J, Schramme MC, Schumacher J, DeGraves FJ. Diagnostic analgesia of
527 the equine digit. *Equine Vet Educ.* 2013;25:408-21.

528 [41] Ross MW. Subchondral Bone Pain – The Fetlock Joint in Racehorses and Sports
529 Horses. American Association of Equine Practitioners Orlando, USA. 2016. p. 58-64.

530 [42] Young BD, Samii VF, Mattoon JS, Weisbrode SE, Bertone AL. Subchondral bone
531 density and cartilage degeneration patterns in osteoarthritic metacarpal condyles of
532 horses. *Am J Vet Res.* 2007;68:841-9.

533 [43] Schramme M, Schumacher J, Schumacher J. Clinical examination, differential
534 analgesia and imaging modalities for the investigation of distal limb lameness. Lameness
535 and Imaging - American Association of Equine Practitioners Focus Meeting. Fort Collins,
536 Colorado, USA. 2007. p. 51-69.

537 [44] Bienert A, Stadler P. Computed tomographic examination of the locomotor
538 apparatus of horses - a review. *Pferdeheilkunde.* 2006;22:218.

539 [45] Nsoor N. Factors That Can Be Attributable to Radiation Dose Reduction among
540 Pediatric Age Group Undergoing Brain Computed Tomography. *Pak J Med Sci.*
541 2009;25:669-73.

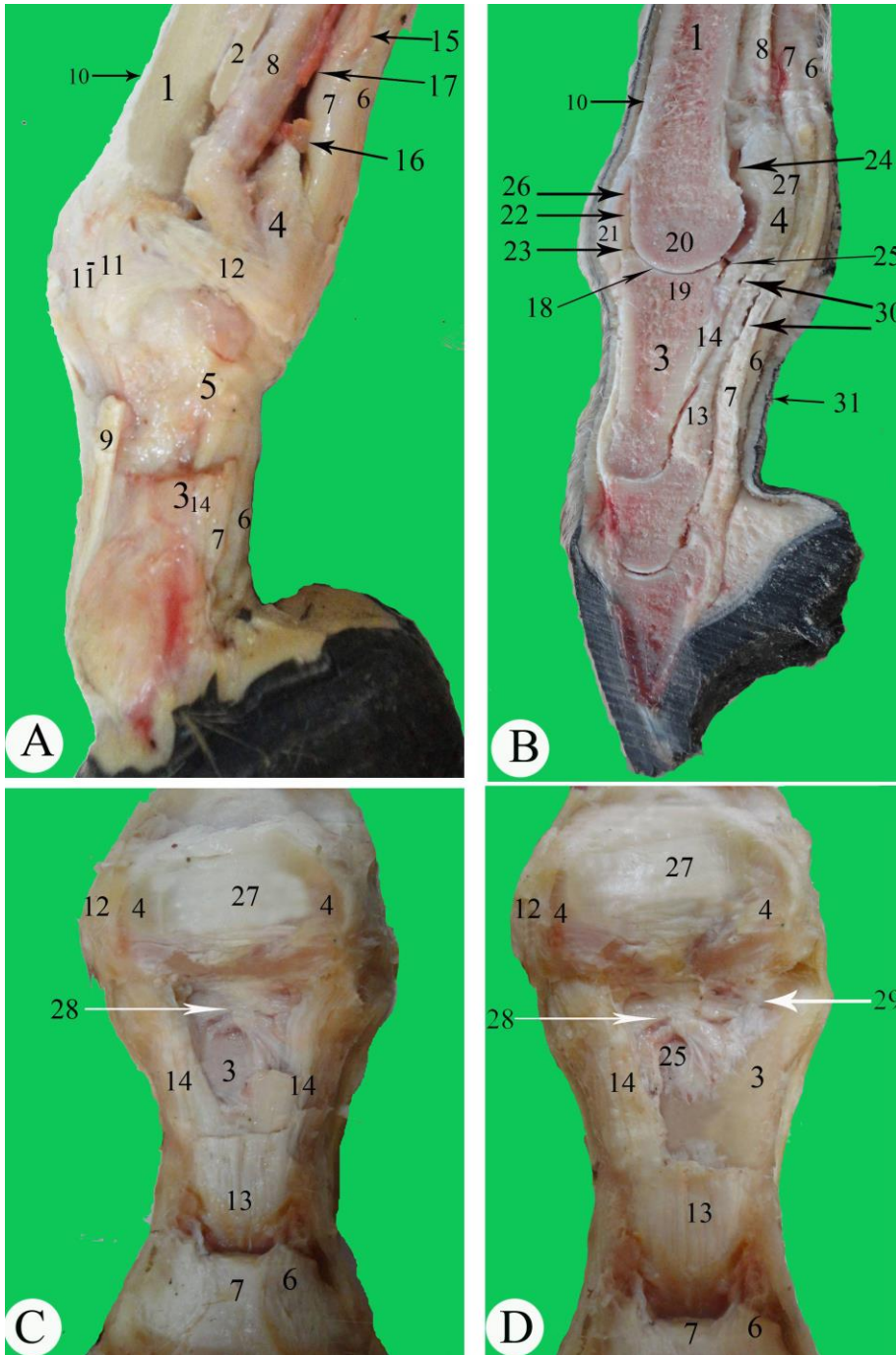
542 [46] Kalra MK, Blake MA, Maher MM. Does low dose abdominal-pelvic CT compromise
543 the lesion detection and morphological appearance? *Am J Roentgenol.* 2003;180:8.

544 [47] Kalra MK, Maher MM, Toth TL, Schmidt B, Westerman BL, Morgan HT, et al.
545 Techniques and applications of automatic tube current modulation for CT. *Radiology*.
546 2004;233:649-57.
547 [48] Li F, Sone S, Abe H, MacMahon H, Armato SG, Doi K. Lung cancers missed at low-
548 dose helical CT screening in a general population: Comparison of clinical,
549 histopathologic, and imaging findings. *Radiology*. 2002;225:673-83.
550 [49] Rehani MM, Bongartz G, Kalender W, Golding SJ, Gordon L, Murakami T, et al.
551 Managing x-ray dose in computed tomography: ICRP special task force report. *Ann ICRP*
552 2000:7-45.
553 [50] Kovac M, Litvin YA, Aliev RO, Zakirova EY, Rutland CS, Kiyasov AP, et al. Gene
554 Therapy Using Plasmid DNA Encoding Vascular Endothelial Growth Factor 164 and
555 Fibroblast Growth Factor 2 Genes for the Treatment of Horse Tendinitis and Desmitis:
556 Case Reports. *Front Vet Sci*. 2017;4:168.
557
558

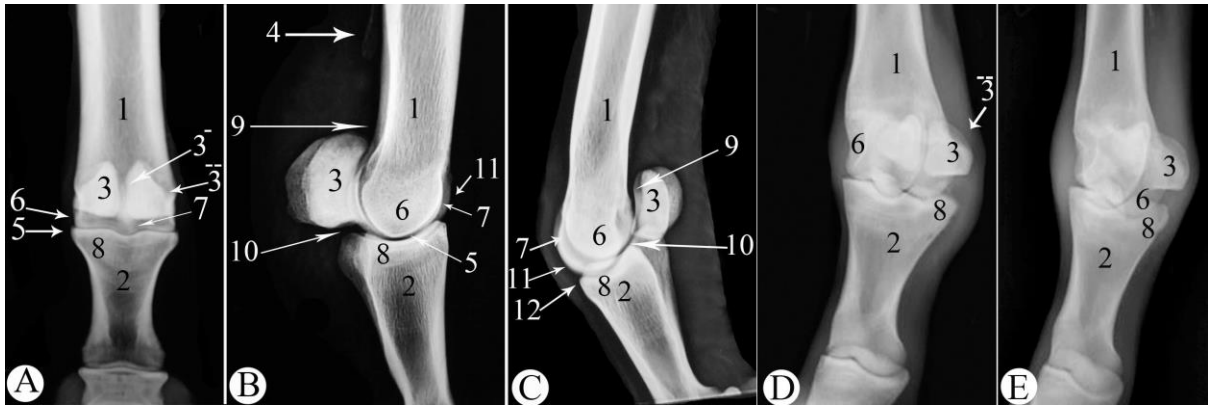
559 Table 1. Donkey Specimens

Donkey identification number	Age (years)	Sex	Condition	X-ray	Computed tomography	Anatomical dissection and cast
1	5	Male	Healthy	X	X	
2	5	Male	Healthy	X	X	X
3	8	Female	Healthy	X		X
4	7	Female	Healthy	X		
5	7	Male	Healthy	X		
6	7	Male	Affected	X	X	
7	5	Male	Affected	X	X	
8	5	Male	Affected	X	X	
9	7	Female	Affected	X	X	
10	8	Female	Affected	X	X	
11	5	Male	Healthy			X
12	6	Male	Healthy			X
13	7	Male	Healthy			

560
561

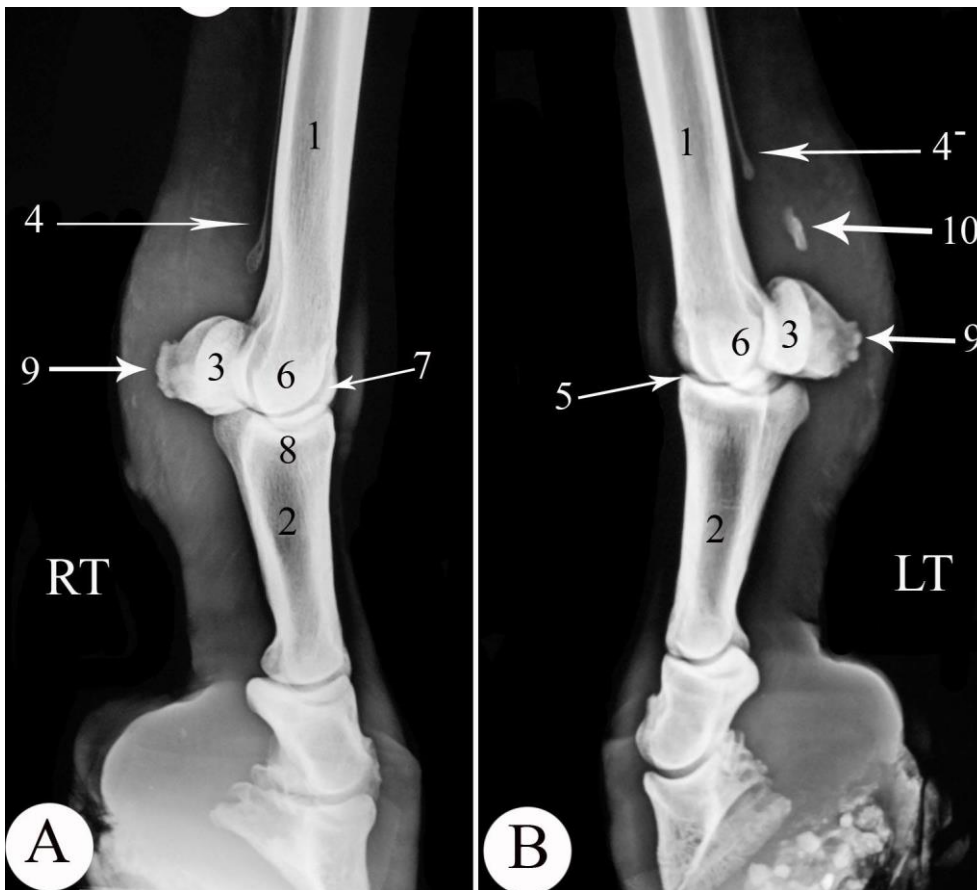


562
 563 Fig.1. Anatomical dissection of metatarsophalangeal joint. (A) Medial, (B) sagittal and (C-D)
 564 plantar views. 1-Third metatarsal bone. 2-Second metatarsal bone. 3-Proximal phalanx. 4-
 565 Proximal sesamoid bone. 5-Proximal digital annular ligament. 6-Superficial digital flexor
 566 tendon. 7-Deep digital flexor tendon. 8-Suspensory ligament. 9-Extensor branch of
 567 suspensory (dissected). 10-Long digital extensor tendon. 11-Collateral ligament of the joint
 568 (superficial+deep). 12-Medial collateral sesamoidean ligament. 13-Straight sesamoidean
 569 ligament. 14-Oblique sesamoidean ligament. 15-Medial plantar nerve. 16-Lateral dorsal
 570 metatarsal artery. 17-Plantar vein. 18-Joint cavity. 20-Metatarsal condyle. 21-Dorsal capsule
 571 of the joint. 22-Dorsal recess. 23-Distodorsal recess. 24-Proximal plantar recess. 25-Distal
 572 plantar recess. 26-Plica synovialis. 27-Intersesamoidean ligament. 28-Cruciate sesamoidean
 573 ligaments. 29-Short sesamoidean ligament. 30-Synovial digital sheath cavity. 31-Skin.
 574
 575



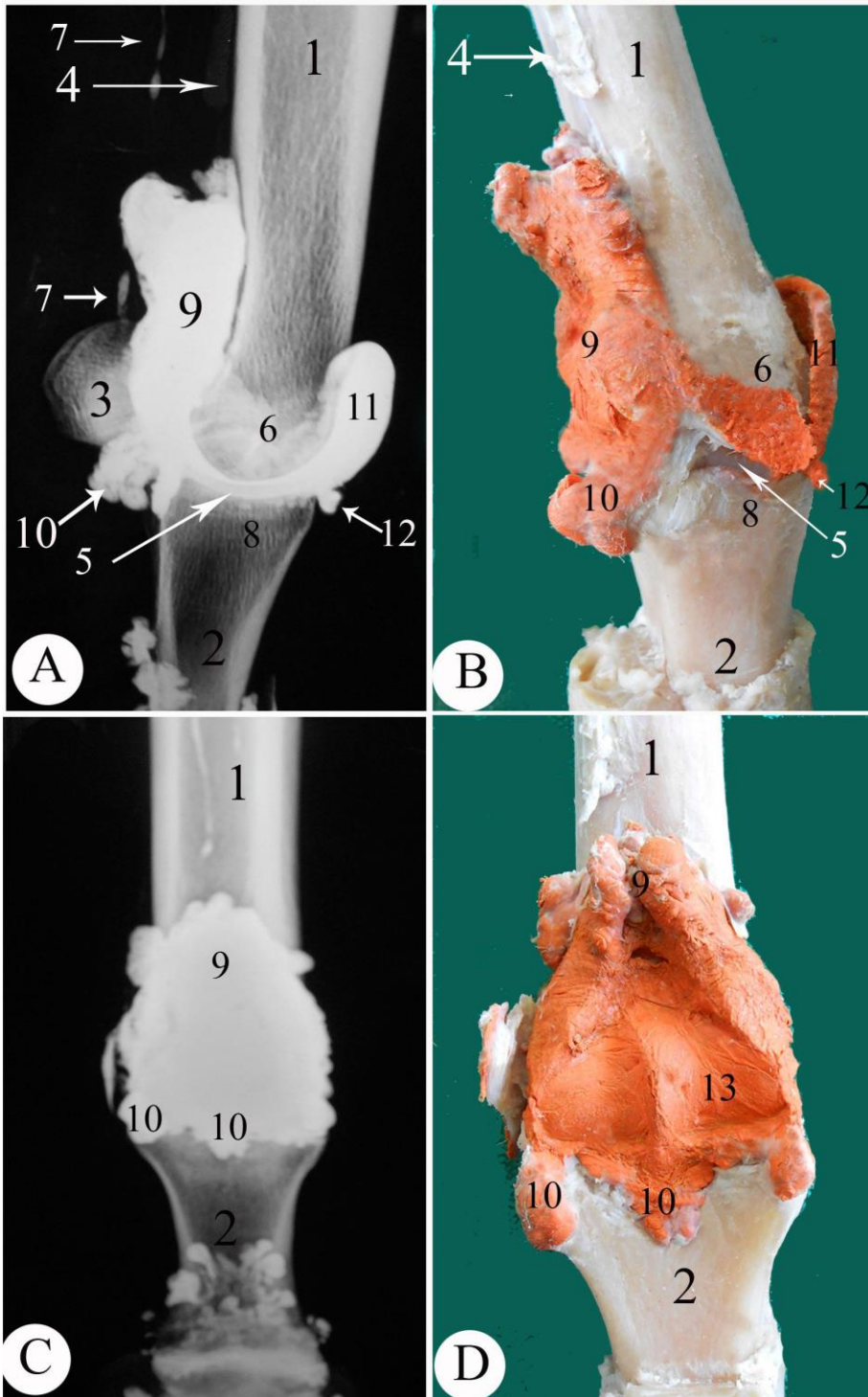
576
577
578
579
580
581
582
583

Fig. 2. Normal radiographic appearance of the metacarpophalangeal joint; (A) Dorsopalmar, (B) Lateromedial, (C) Oblique flexed lateromedial, (D) Dorsolateral-palmaromedial oblique, (E) Dorsomedial-palmarolateral oblique. 1-Third metacarpal bone. 2-Proximal phalanx. 3-Proximal sesamoid bone. 3^aaxial border. 3^babaxial border. 4-Second/fourth metacarpal bone. 5-Joint cavity. 6+7-Condyle of the third metacarpal bone. 9-proximal-palmar recess. 10-Distal-palmar recess. 11-Dorsal recess. 12-Distodorsal recess.



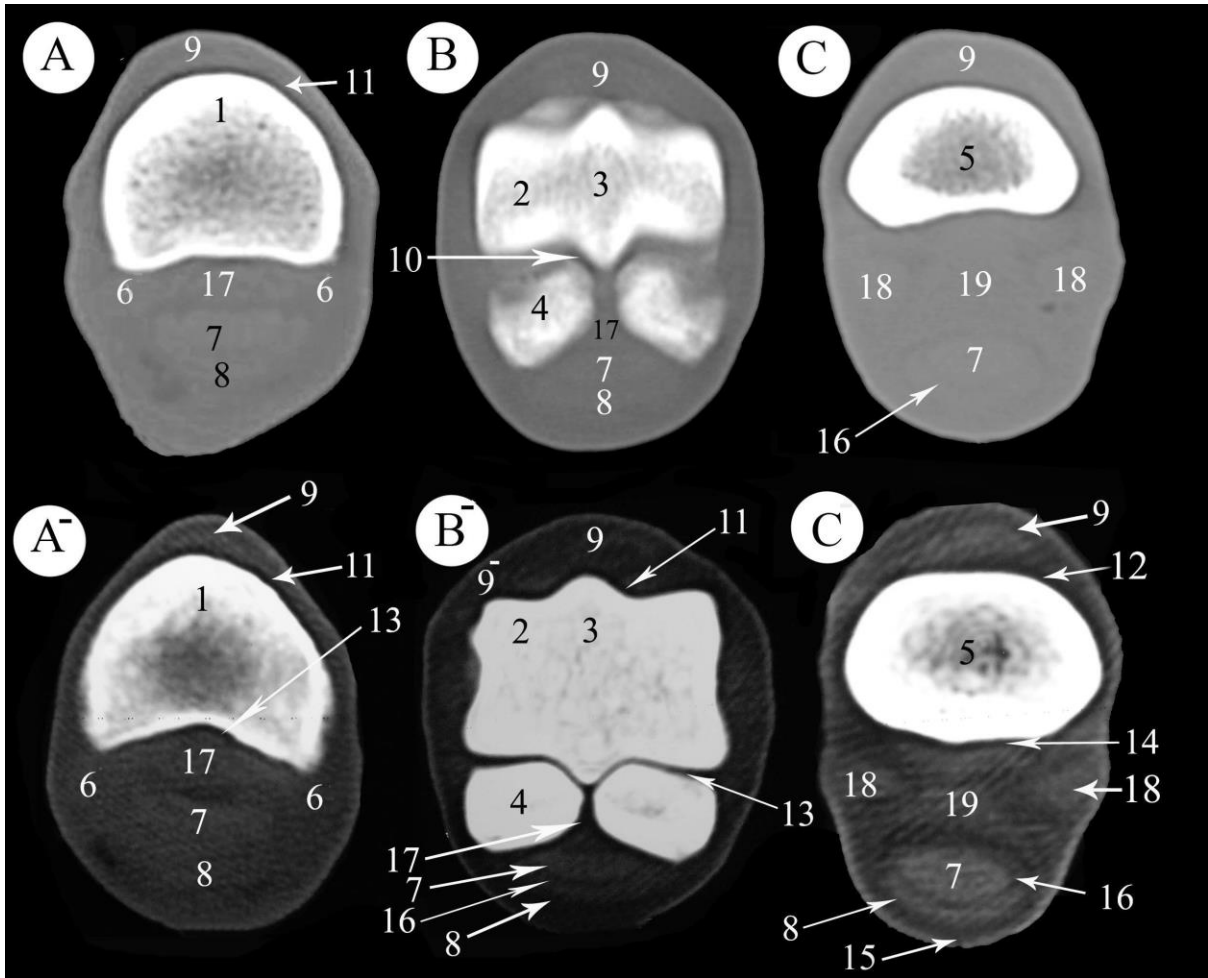
584
585
586
587
588
589
590
591
592

Fig. 3. New bone proliferations on the palmar margin of the proximal sesamoid bones and calcification of the lateral branch of the suspensory ligament. Oblique views of right (A) and left (B) metacarpophalangeal joint; 1-Third metacarpal bone. 2-Proximal phalanx. 3-Proximal sesamoid bone. 4 and 4- -Second and fourth metacarpal bone, cannot be differentiated given the view. 5-Joint cavity. 6-Condyles of third metacarpal. 7-Sagittal crest. 9-Bony exostosis. 10-Calcification of suspensory ligament lateral branch.



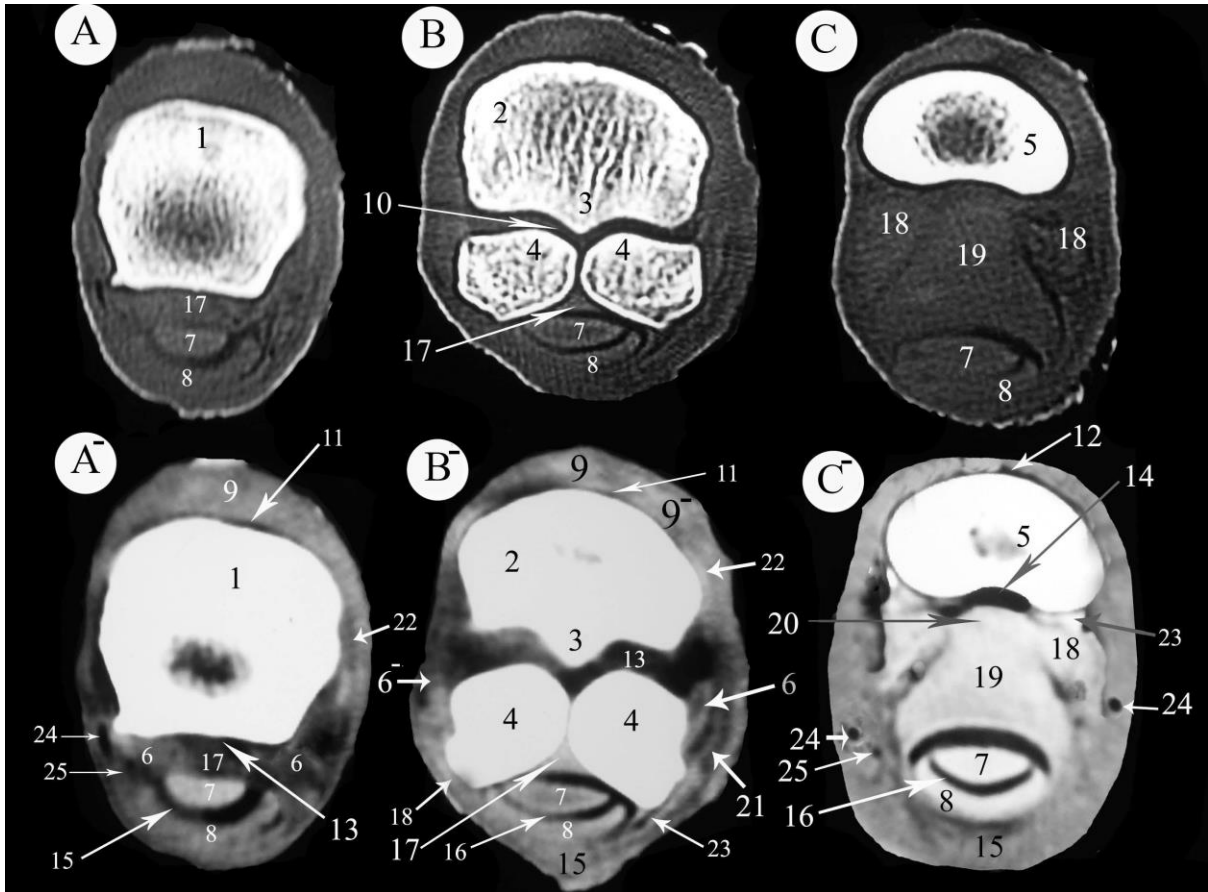
593
 594 Fig. 4. Contrast radiographic and dissected cast images of the metacarpophalangeal joint,
 595 possibly with a distended joint and marked synovial proliferations. . (A) Lateromedial
 596 contrast radiograph. (B) Lateral view of dissected cast. (C) Dorsopalmar contrast radiograph.
 597 (D) Palmar view of dissected cast. 1-Third metacarpal bone. 2-Proximal phalanx. 3-Proximal
 598 sesamoid bone. 4-Distal end of the second metacarpal bone 5-Joint cavity. 6-Condyle of
 599 metacarpal. 7-Digital sheath or possible mineralization of the tendon. 9-Proximal-palmar
 600 recess. 10-Distal-palmar recess. 11-Dorsal recess. 12-Distodorsal recess. 13-Impression of
 601 proximal part of the sesamoid bone.

602
 603



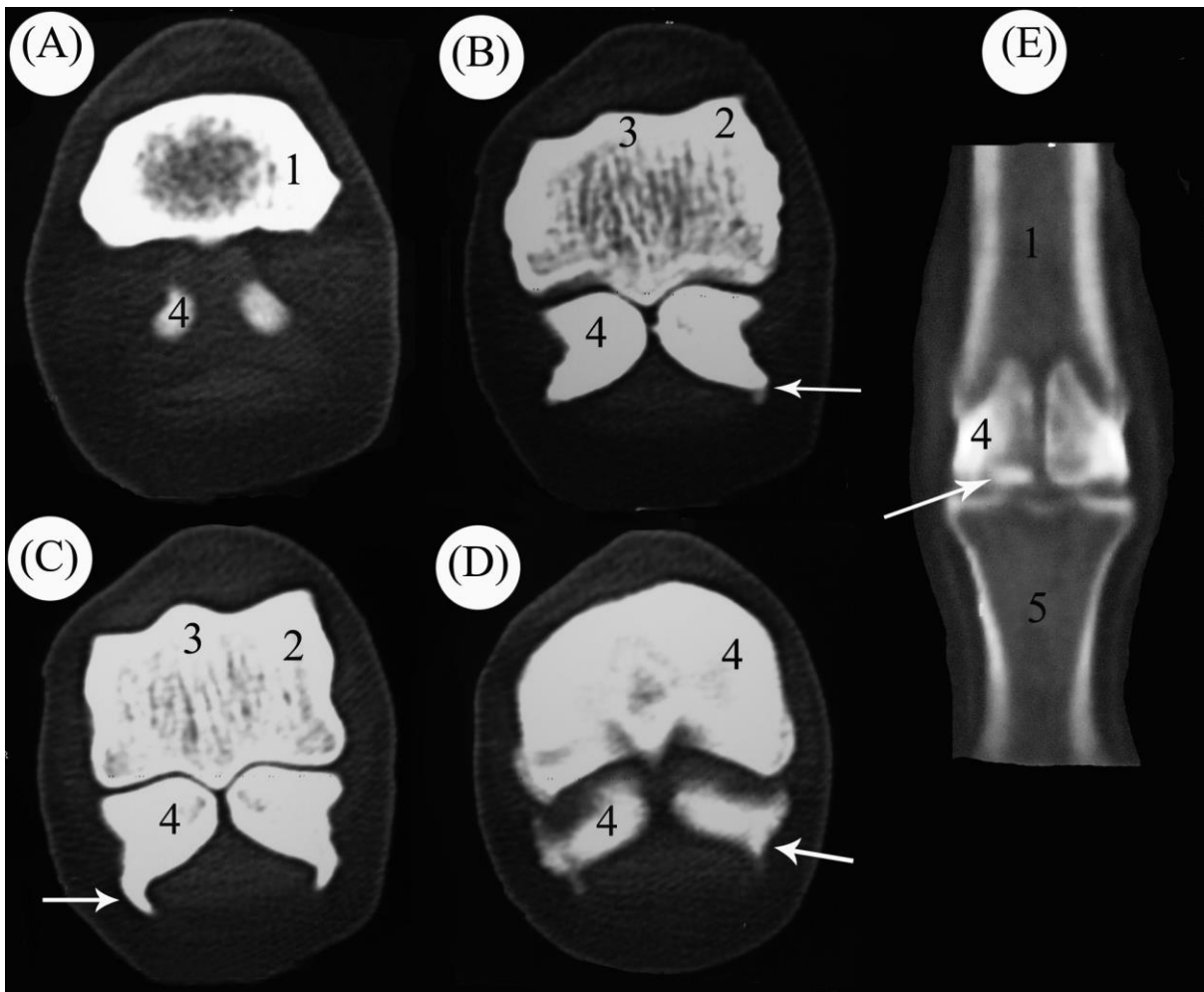
604
 605
 606
 607
 608

Fig. 5. Transverse computed tomography of the normal metacarpophalangeal joint at 110kV, 120mA. At the levels A) proximal to sesamoid bone, B) sesamoid bone, C) distal to sesamoid bone.



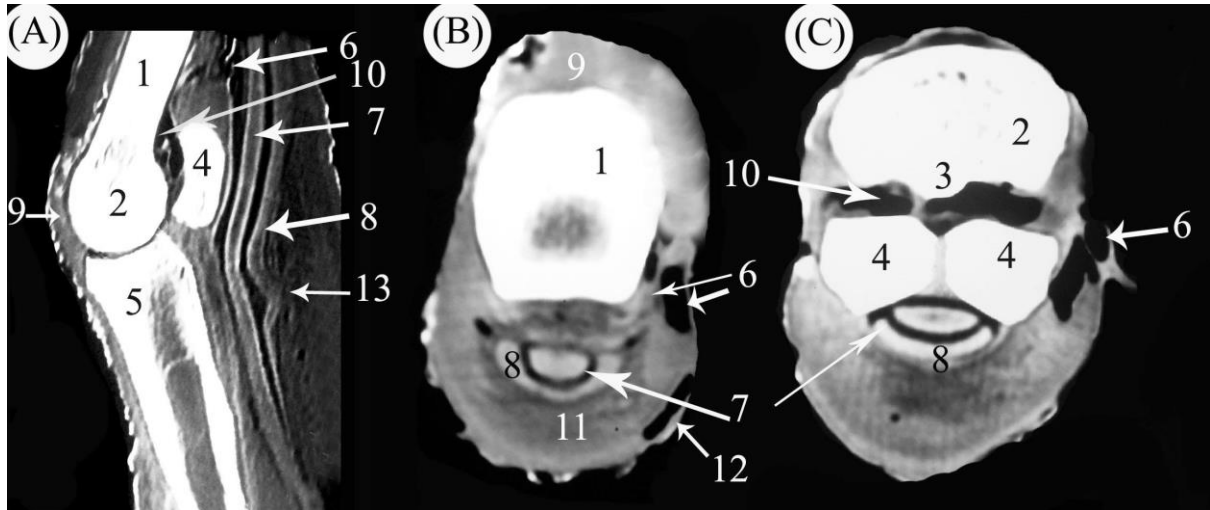
609
 610
 611
 612
 613

Fig. 6. Transverse Computed tomography of healthy metacarpophalangeal joint at 120kV, 300mA. Level A) proximal to sesamoid bone, B) sesamoid bone, C) distal to sesamoid bone.



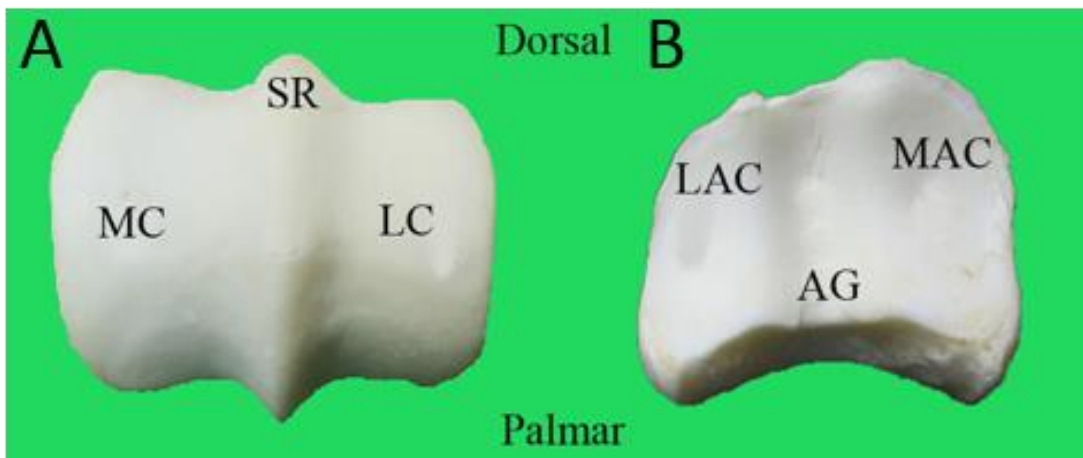
614
 615 Fig. 7. Computed tomography of abnormal metacarpophalangeal joint from a transverse view
 616 (A-D) and dorsopalmar view radiograph (E) showing the bony projection (exostosis). 1-Third
 617 metacarpal bone. 2-Condyle of third metacarpal bone. 3-Sagittal ridge of third metacarpal
 618 bone. 4-Proximal sesamoid bone. 5-Proximal phalanx and bony extension (arrow).
 619

620



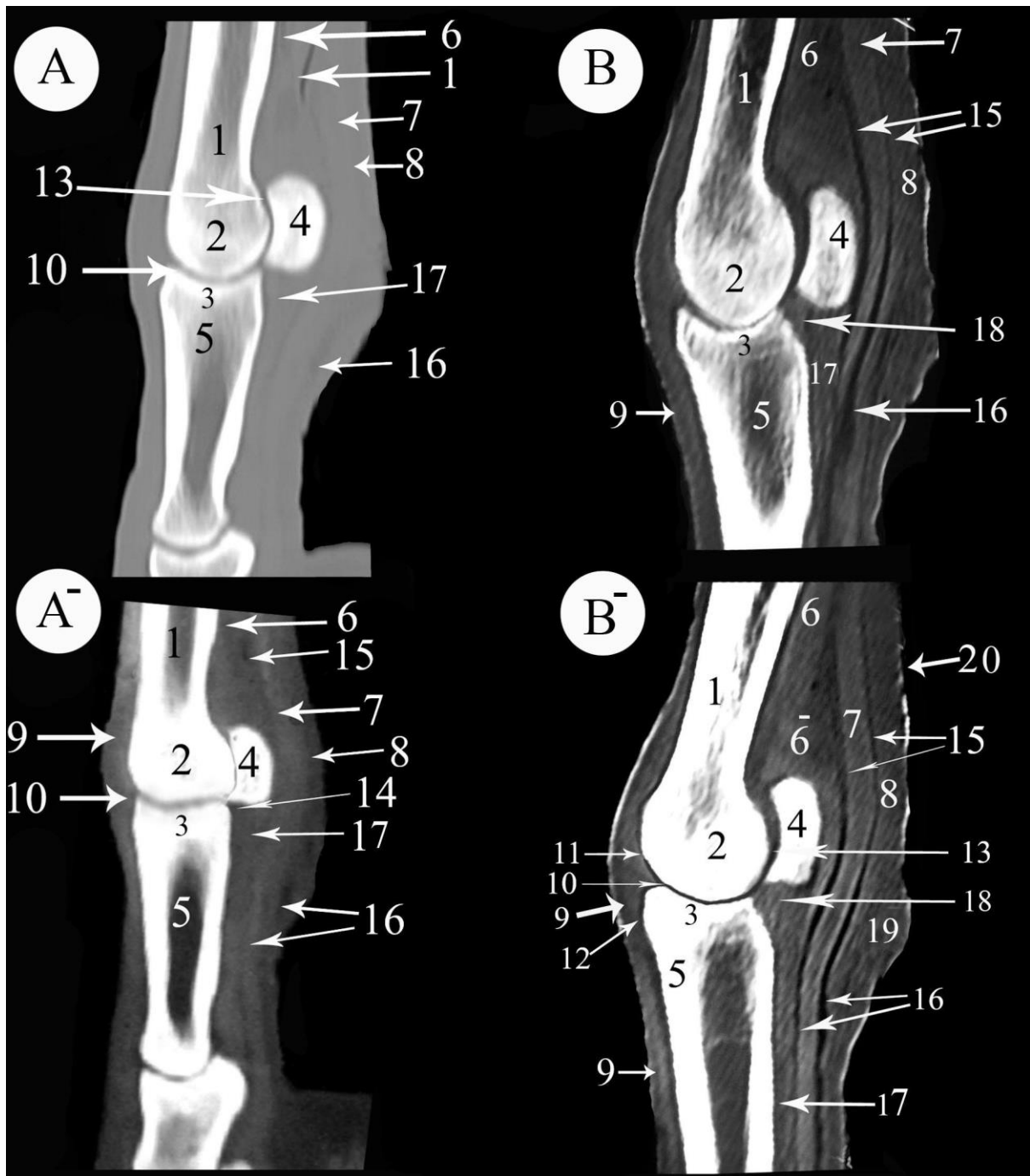
621
622
623
624
625
626
627
628
629
630

Fig. 8. Computed tomography of the abnormal metatarsophalangeal joint. Sagittal (A) and transverse views (B and C) soft window at 120kV, 300mA. At levels B) distal to the fetlock C) at sesamoid bone. 1-Third metacarpal bone. 2-Condyle of third metacarpal bone. 3-Sagittal ridge of third metacarpal bone. 4-Proximal sesamoid bone. 5-Proximal phalanx. 6-Note change of density and appearance of gas), 7-Deep digital flexor tendon. 8-Superficial digital flexor tendon. 9-Dorsal digital extensor tendon. 10-Joint cavity (note increase in size, appearance of hyperdense septa or structures). 11-Ergot cushion. 12-Fluid at the lateral part of the cushion. 13-Sigmoid shape of superficial digital flexor tendon.



631
632
633
634
635
636

Supplemental Figure 1. Anatomical bone specimen. A) Distal extremity of third metacarpal bone. MC-medial condyle. LC-lateral condyle. SR-sagittal ridge. B) Proximal extremity of proximal phalanx. MAC-medial articular cavity. AG-sagittal groove. LAC-lateral articular cavity.



637
 638 Supplemental Figure 2. Parasagittal Computed tomography of the normal
 639 metacarpophalangeal joint. A+B) are bone window and A⁻+B⁻) are soft window. (A +A⁻) at
 640 120kV, 120mA, while B+B⁻) 120kV, 300mA. 1-Third metacarpal bone. 2-Condyle of 3rd
 641 metacarpal bone. 3-Articular cavity of proximal phalanx. 4-Proximal sesamoid bone. 5-
 642 Proximal phalanx. 6-Suspensory ligament. 6⁻Branches of suspensory ligaments. 7-Deep
 643 digital flexor tendon. 8-Superficial digital flexor tendon. 9-Common digital extensor
 644 tendon.10-Joint cavity. 11-Dorsal recess. 12-Distodorsal recess. 13-Palmaroproximal recess.
 645 14-Palmarodistalrecess. 15-Proximal digital sheath cavity. 16-Distal digital sheath cavity. 17-
 646 Straight sesamoidean ligament. 18- Cruciate sesamoidean ligaments. 19- Ergot cushion. 20-
 647 Skin.